International Journal of Innovative Research and Scientific Studies, 8(6) 2025, pages: 1147-1161

IJIRSS
International Journal of Innovative Research & Scientific Studies

ISSN: 2617-6548

URL: www.ijirss.com

A physical and mathematical model of the melt motion at the SCR process equipment

Kazhikenova Saule

The Higher Mathematics Department Abylkas Saginov Karaganda Technical University, Kazakhstan.

(*Email: sauleshka555@mail.ru*)

Abstract

The primary objective of this study is to develop a physical and mathematical model of melt hydrodynamics to enhance the understanding of the structural and physical properties of molten systems. The mathematical modeling of hydrodynamic processes is based on the Navier-Stokes equations. To obtain a priori estimates, the Galerkin approach was applied to transfer the limit, enabling the numerical solution of the Navier-Stokes equations with appropriate boundary conditions. A mathematical model describing the incompressible melt motion within a limited area was developed. Additionally, a computer program was created for the numerical solution of the hydrodynamic equations. An algorithm was also developed to construct the distribution of flow rates in molten systems based on numerical experiments. A physical and mathematical model of the incompressible melt motion was specifically constructed for the continuous rolling lines of «Kazakhmys Corporation» LLP used for copper rods. During the hot continuous rolling of copper alloys, the issue of copper sticking to the chute significantly impacts the quality of the final copper products. This study addresses the problem of copper sticking during the hot rolling process by investigating key technologies aimed at improving the production line process of copper rods.

Keywords: Copper rod, Hydrodynamics, Melt's motion, Numerical modelling.

DOI: 10.53894/ijirss.v8i6.9829
Funding: This work is supported by the Science Committee of the Higher Education and Science Ministry of the Republic of Kazakhstan, Kazakhstan (Grant number: AP23486482).
History: Received: 21 July 2025 / **Revised:** 25 August 2025 / **Accepted:** 27 August 2025 / **Published:** 12 September 2025

Competing Interests: The authors declare that they have no competing interests.
Authors' Contributions: SK designed and implemented the study, analyzed the results, and wrote the manuscript.
Transparency: The authors confirm that the manuscript is an honest, accurate, and transparent account of the study; that no vital features of the study have been omitted; and that any discrepancies from the study as planned have been explained. This study followed all ethical practices during writing.
Institutional Review Board Statement: The Ethical Committee of Abylkas Saginov Karaganda Technical University, Kazakhstan, has granted approval for this study.
Publisher: Innovative Research Publishing

1. Introduction

The physical and mathematical model of the hydrodynamic equations is presented, for the study of which special attention is paid to the study of melt viscosity, since viscosity is closely related to the physical parameters of the melt [1-4].

The issue of meeting the needs of the domestic industry with high-quality products has necessitated the development of scientific foundations and methods for studying the thermophysical and structural properties of metal melts. Conducting metallurgical experiments is expensive and difficult. Numerical simulations are the simplest and most effective way to evaluate the furnace processes. Scientific research in these areas has made it possible to find solutions to the numerous problems associated with molten systems.

In this regard, the relevance of this study is determined by the objective and urgent need to develop nonstationary physical and mathematical models of the structural properties of molten metals. Numerical solutions of the Navier-Stokes equations have been used in many practical applications and scientific papers. However, in analytical form, solutions of these equations have been found only in some special cases; therefore, there is no complete understanding of the properties of the Navier-Stokes equations [5].

In particular, solutions to the Navier-Stokes equations often include turbulence, which remains one of the most important unsolved problems in physics despite its enormous importance in science and technology [6-9].

Simulation of incompressible flow inside a cubic lid-driven cavity for a range of Reynolds numbers is carried out using the dynamic Smagorinsky model (DSM). The centerline average velocity profiles were compared with existing experimental and numerical results [10]. The Kolmogorov length scale and Taylor microscale were calculated, and it was found that both decreased towards the wall as dissipation was high at the walls.

The application of direct numerical simulations and fully three-dimensional linear stability analyses is investigated, «increasing the Reynolds number triggers self-sustained periodic oscillations of the flow in the vicinity of the spanwise end walls of the cavity» [11]. Mathematical models of microstructure were established based on the cellular automaton-finite difference (CA-FD). The simulated and experimental results were compared in this study, and they agreed well [12].

Mathematical models that reduce the equation to a system of two ordinary differential equations were defined. It was shown that constructing exact solutions reduces the integration of a system of linear equations with arbitrary predefined functions [13].

Several strategies have been proposed to improve nonlinear systems [14-25]. The theory of the Navier-Stokes equations is very rich in its content, and its development poses new mathematical problems related not only to applications in hydrodynamics but also in areas of fundamental mathematics such as the theory of embedding of functional spaces, potential theory, and interpolation theory.

The variational multiscale framework for the finite element approximation of the compressible Navier-Stokes equations written in the conservation form is given [20].

Among the calculated volumes of fluid flow, one can distinguish closed volumes of fluid flow that do not exchange flow with neighboring volumes; these are known as closed systems. These systems are limited by impermeable walls or surfaces under known pressure, free surfaces, or generating surfaces through which the flow passes with a known velocity. The systems described by the Navier-Stokes equations, with specific boundary conditions such as pressures or velocities at all boundaries, are considered closed. The solution to the Navier-Stokes equations can always be obtained from the modified Navier-Stokes equations. Therefore, for closed systems, a global solution to the Navier-Stokes equations always exists. This study solves the solution to the Navier-Stokes equations by applying a small parameter to modify it, approximating the equations using this small parameter, and applying Galerkin's method to construct approximate solutions.

2. Methods. Problem Statement

Let us consider the following system of nonlinear stationary equations representing a mathematical model of the motion of an incompressible melt in a limited area $Q \in R^3$ with a smooth border $\Gamma = \partial Q$:

$$\begin{cases} (\rho\upsilon\cdot\nabla)\upsilon = \gamma\Delta\upsilon - \nabla p + \kappa(\nabla\rho\cdot\nabla)\upsilon + \kappa(\upsilon\cdot\nabla)\nabla\rho - \kappa^2 div\left(\left(\frac{1}{\rho}\cdot\nabla\rho\cdot\nabla\right)\rho\right) + \rho g, \\ (\upsilon\cdot\nabla)\rho = \kappa\Delta\rho, \\ div\upsilon = 0, \end{cases} \quad (1)$$

with boundary conditions:

$$\upsilon\big|_\Gamma = 0, \quad \rho\big|_\Gamma = \rho_\Gamma(x), \quad (2)$$

$\upsilon(x) = \upsilon(x_1, x_2, x_3)$ is the velocity; $\rho(x) = \rho(x_1, x_2, x_3)$ is the density; $p(x) = p(x_1, x_2, x_3)$ is the pressure; $g(x) = g(x_1, x_2, x_3)$ is the mass, and κ, γ are the diffusion and viscosity coefficients.

If the velocity has a component normal to the wall, the wall receives energy from the liquid and completely returns it to the liquid (changing the direction of the velocity). The tangential component of the velocity is zero (adhesion effect). Therefore, these walls do not change the energy of the system. However, the energy reflected from the walls creates an internal energy flow that circulates between the walls. Thus, in this case, all of the above formulas remain unchanged, but the conditions on the walls (impermeability and adhesion) should not be formulated explicitly; they appear as a result of

solving the problem during integration in the region limited by the walls. To implement this method, it is sufficient to describe the boundaries of the closed region in which the solution is considered. There is also no need to supplement these equations with boundary conditions because the boundaries can be walls or free surfaces. This proof was based on the fact that the fluid did not change. The solvability of problems (1) and (2) in [6].

This paper proposes a function approximation using a small parameter that combines two forms of boundary value problems for hydrodynamic equations. The computation of an approximate value function from an approximate model is shown to be equivalent to the computation of the exact value function for a finite model derived from data. It is known that the system in Equation 1 is not a Cauchy-Kovalevskaya system. Note that the Cauchy-Kovalevskaya theorem also plays an important role in the study of hydrodynamic equations [7]. Estimates that guarantee the stability of the solution exist for solutions of the Cauchy problem as well as boundary value problems for hydrodynamic equations. The approximate solutions of systems (1) and (2) can be obtained by approximating the equation coefficients, free terms, and initial functions using a small parameter. The convergence of the approximate solutions to the exact solution of the Navier-Stokes equations follows from energy estimates.

Let us construct a system of Equations (3) – (4), which is an approximation of the original models (1) – (2) with a small parameter $\varepsilon \quad (\varepsilon > 0)$:

$$\begin{cases} (\rho^\varepsilon \upsilon^\varepsilon \cdot \nabla)\upsilon^\varepsilon = \gamma \Delta \upsilon^\varepsilon - \nabla p^\varepsilon + \kappa(\nabla \rho^\varepsilon \cdot \nabla)\upsilon^\varepsilon + \kappa(\upsilon^\varepsilon \cdot \nabla)\nabla \rho^\varepsilon - \kappa^2 div\left(\left(\frac{1}{\rho^\varepsilon}\cdot\nabla\rho^\varepsilon\cdot\nabla\right)\rho^\varepsilon\right) + \rho^\varepsilon g - \frac{1}{2}\rho^\varepsilon \upsilon^\varepsilon div\upsilon^\varepsilon, \\ (\upsilon^\varepsilon \cdot \nabla)\rho = \kappa\Delta\rho^\varepsilon, \\ \varepsilon p^\varepsilon + div\upsilon^\varepsilon = 0 \end{cases} \tag{3}$$

$$\upsilon^\varepsilon\big|_\Gamma = 0, \quad \rho^\varepsilon\big|_\Gamma = \rho_\Gamma(x). \tag{4}$$

The system of Equations 3 is a Cauchy-Kovalevskaya type system.

Definition. The set of functions $\{\upsilon^\varepsilon(x), \rho^\varepsilon(x), p^\varepsilon(x)\}$ is called a strongly generalized solution to problems (3) – (4), and satisfies the following conditions:

1) $\upsilon^\varepsilon(x) \in \overset{0}{W}{}_2^1(Q)$, $\rho^\varepsilon \in W_2^2(Q)$, $0 < b \le \rho^\varepsilon(x) \le B < \infty$;

2) $\forall \psi(x) \in \overset{0}{W}{}_2^1(Q)$ integral equal:

$$\int_Q \Big\{\rho^\varepsilon(\upsilon^\varepsilon\cdot\nabla)\psi^\varepsilon\upsilon^\varepsilon - \gamma(\nabla\upsilon^\varepsilon,\nabla\psi) - \kappa(\nabla\rho^\varepsilon\cdot\nabla)\psi\cdot\upsilon^\varepsilon + \frac{1}{2}\rho^\varepsilon div\upsilon^\varepsilon(\upsilon^\varepsilon\cdot\psi) -$$

$$-\kappa(\psi\cdot\nabla)\rho^\varepsilon div\upsilon^\varepsilon - \kappa(\upsilon^\varepsilon\cdot\nabla)\psi\cdot\nabla\rho^\varepsilon + p^\varepsilon div\psi + \kappa^2\left(\left(\frac{1}{\rho^\varepsilon}\cdot\nabla\rho^\varepsilon\cdot\nabla\right)\rho^\varepsilon\right)\nabla\psi - \rho^\varepsilon g\psi\Big\}dx = 0,$$

3) Equations (3) – (4) are fulfilled almost everywhere in Q as appropriate.

R^n is a Euclidean space; $L_2(Q)$ is a Hilbert space; $L_p(Q)$, $1 \le p \le 6$ is a Banach space; $W_2^1(Q)$ is a space consisting of $L_2(Q)$ elements, having squarely summable over *Q* generalized first order derivatives; $W_2^2(Q)$ is a space consisting of elements $L_2(Q)$, having squarely summable over *Q* generalized derivatives of the first and second orders; space $\overset{0}{W}{}_2^1(Q)$ is subspace $W_2^1(Q)$, and is the closure of an infinitely differentiable finite vector function set [5-7].

The system of Equations 3 is a Cauchy-Kovalevskaya system.

Assertion 1. *Let the functions* g, ρ_Γ and κ *is a sufficiently small number, satisfies the conditions*: $g \in \underset{\frac{6}{5}}{L_6}(Q)$, $\rho_\Gamma \in W_2^{3/2}(Q)$, $\kappa \le \delta = \min\left\{\frac{B}{16}\frac{b^2}{C_1b^2 + C_2B^2}, \frac{b}{B-b}\right\}$. *Then there exists at least one strongly generalized solution of the Equations system (3) - (4), where* C_1, C_2 *are constants that depends only on the problem data and do not depend on the* υ^ε, ρ^ε, p^ε *functions.*

Proof. The proof of this assertion 1 consists of three stages:

1) obtaining a priori estimates,
2) using Galerkin's method [19-24],
3) transferring the limit.

1) We obtain the necessary a priori estimates. Let multiply the second Equations 3 by $\Delta\rho^{\varepsilon}(x)$ the scalar in $L_2(Q)$:

$$\kappa\left\|\Delta\rho^{\varepsilon}\right\|^2_{L_2(Q)} = \int_Q \left(\upsilon^{\varepsilon}\cdot\Delta\right)\rho^{\varepsilon}\cdot\Delta\rho^{\varepsilon}dx, \tag{5}$$

After integration in parts is applicable to the right side:

$$\int_Q \left\{\upsilon^{\varepsilon}\cdot\nabla\right\}\rho^{\varepsilon}\cdot\Delta\rho^{\varepsilon}dx = \int_Q \nabla\left(\left(\upsilon^{\varepsilon}\cdot\nabla\right)\rho^{\varepsilon}\right)\cdot\nabla\rho^{\varepsilon}dx + \int_\Gamma \left(\upsilon^{\varepsilon}\cdot\nabla\right)\rho^{\varepsilon}\frac{\partial\rho^{\varepsilon}}{\partial n}d\Gamma = -\int_Q \left(\nabla\upsilon^{\varepsilon}\cdot\nabla\right)\rho^{\varepsilon}\cdot\nabla\rho^{\varepsilon}dx -$$

$$-\frac{1}{2}\int_Q \left(\upsilon^{\varepsilon}\cdot\nabla\right)\left|\Delta\rho^{\varepsilon}\right|^2 dx \le C\left\|\upsilon_x^{\varepsilon}\right\|\cdot\left\|\nabla\rho^{\varepsilon}\right\|^2 \le C\left\|\upsilon_x^{\varepsilon}\right\|\left(\left\|\rho^{\varepsilon}\right\| + \max\left|\rho^{\varepsilon}\right|\cdot\left\|\Delta\rho^{\varepsilon}\right\|\right),$$

the Maximum Principle to the second equation of system (3) is $\exists b, 0 < b \le \rho^{\varepsilon}(x) \le B < \infty$;

then:

$$\int_Q \left\{\upsilon^{\varepsilon}\cdot\nabla\right\}\rho^{\varepsilon}\cdot\Delta\rho^{\varepsilon}dx \le \left\|\upsilon_x^{\varepsilon}\right\|\left(C_1 + C_2\left\|\Delta\rho^{\varepsilon}\right\|\right) \le \alpha\left\|\Delta\rho_x^{\varepsilon}\right\|^2 + C(\alpha)\left(\left\|\upsilon_x^{\varepsilon}\right\|\right) + C.$$

If $\alpha = \frac{\kappa}{2}$, then from Equation 5 follows inequality (6):

$$\frac{\kappa}{2}\left\|\Delta\rho^{\varepsilon}\right\|^2 \le C(\kappa)\left\|\upsilon_x^{\varepsilon}\right\|^2 + C. \tag{6}$$

Let multiply the third equation in (3) by the function $\upsilon^{\varepsilon}(x)$ scalar in space $C_2(Q)$:

$$\frac{1}{2}\int_Q \left(\rho^{\varepsilon}\upsilon^{\varepsilon}\cdot\nabla\right)\left|\upsilon^{\varepsilon}\right|^2 dx + \gamma\left\|\upsilon_x^{\varepsilon}\right\|^2 = \int_Q \rho^{\varepsilon} g\upsilon^{\varepsilon}dx + \int_Q p^{\varepsilon} div\upsilon^{\varepsilon}dx + \frac{\kappa}{2}\int_\Omega \left(\nabla\rho^{\varepsilon}\cdot\nabla\right)\left|\upsilon^{\varepsilon}\right|^2 dx +$$

$$+\kappa\int_Q \left(\upsilon^{\varepsilon}\cdot\nabla\right)\nabla\rho^{\varepsilon}\cdot\upsilon^{\varepsilon}dx + \kappa^2\int_Q \left(\frac{1}{\rho^{\varepsilon}}\cdot\nabla\rho^{\varepsilon}\cdot\nabla\right)\rho^{\varepsilon}\cdot\nabla\upsilon^{\varepsilon}dx.$$

$$\gamma\left\|\upsilon_x^{\varepsilon}\right\|^2_{C_2(Q)} + \frac{1}{\varepsilon}\left\|div\upsilon^{\varepsilon}\right\|^2_{C_2(Q)} = \int_Q \left\{-\kappa\left(\upsilon^{\varepsilon}\cdot\nabla\right)\upsilon^{\varepsilon}\cdot\nabla\rho^{\varepsilon} + \kappa\left(\upsilon^2\cdot\nabla\right)\rho^{\varepsilon}div\upsilon^{\varepsilon}\right\}dx +$$

$$+\int_Q \left\{\kappa^2\left(\left(\frac{1}{\rho^{\varepsilon}}\cdot\nabla\rho^{\varepsilon}\cdot\nabla\right)\rho^{\varepsilon}\right)\cdot\nabla\upsilon^{\varepsilon} + \rho^{\varepsilon}g\upsilon^{\varepsilon}\right\}dx.$$

We obtain a priori estimates of the integral terms in the same manner as in [6]

$$\gamma\left\|\upsilon_x^{\varepsilon}\right\|^2 + \frac{1}{\varepsilon}\left\|div\,\upsilon^{\varepsilon}\right\|^2 \le \frac{\kappa^2}{b}B\left\|\Delta\rho^{\varepsilon}\right\|\cdot\left\|\upsilon_x^{\varepsilon}\right\| + \frac{\kappa^2}{b}\left\|\rho^{\varepsilon}\right\|\cdot\left\|\upsilon_x^{\varepsilon}\right\| + C_1\left\|g\right\|_{L_{\frac{6}{5}}(Q)}\cdot\left\|\upsilon_x^{\varepsilon}\right\| +$$

$$+\kappa\frac{B-b}{2}\left\|\upsilon_x^{\varepsilon}\right\|^2. \tag{7}$$

Let $\gamma - \kappa\frac{B-b}{2} \ge \frac{B}{2}$, and an inequality implies $\kappa \le \frac{B-b}{2}$.

We use repeatedly Jung's inequality to (7), then:

$$\frac{\gamma}{2}\left\|\upsilon_x^{\varepsilon}\right\|^2 + \frac{1}{\varepsilon}\left\|div\,\upsilon^{\varepsilon}\right\|^2 \le \alpha\left\|\Delta\rho\right\|^2 + \frac{B^2}{b^2}\kappa^4 C(\alpha)\left\|\upsilon_x\right\|^2 + \alpha_1\left\|\upsilon_x\right\|^2 +$$

$$+C(\kappa, b, B, \alpha_1) + \frac{\gamma}{4}\left\|\upsilon_x\right\|^2 + C_1(\gamma)\left\|g\right\|^2_{L_{\frac{6}{5}}}. \tag{8}$$

Choose $\alpha = \kappa^3, \alpha_1 = \frac{\gamma}{8}$ and, taking into account (8):

$$\frac{\gamma}{2}\left\|\upsilon_x^\varepsilon\right\|^2 + \frac{1}{\varepsilon}\left\|div\,\upsilon^\varepsilon\right\| \le C\kappa\left\|\upsilon_x\right\|^2 + \kappa^2\left\|\upsilon_x\right\|^2 + C_2\frac{B^2}{b^2} + \kappa\left\|\upsilon_x\right\|^2 + C_1(\mu)\left\|g\right\|_{L_{\frac{6}{5}}}^2 + C.$$

The following inequality are held $\beta \le \frac{\gamma}{32\kappa^2}$, $\beta \le \frac{\gamma}{16}\cdot\frac{b^2}{C_1b^2 + C_2B^2}$, and $\frac{\gamma}{32}\left\|\upsilon_x^\varepsilon\right\|^2 + \frac{C}{\varepsilon}\left\|div\upsilon^\varepsilon\right\|^2 \le C_1(\gamma)\left\|g\right\|_{L_{\frac{6}{5}}}^2 + C.$ The result is a fair assessment (9) for κ smallness (10):

$$\left\|\upsilon_x^\varepsilon\right\|^2 + \frac{1}{\varepsilon}\left\|div\,\upsilon^\varepsilon\right\|^2 \le C < \infty \tag{9}$$

$$\kappa \le \delta = \min\left\{\frac{B}{16}\frac{b^2}{C_1b^2 + C_2B^2}, \frac{b}{B-b}\right\}. \tag{10}$$

From the embedding theorems and from (8), considering (9) it follows that (11) and (12):

$$\upsilon^\varepsilon \in L_p(Q), 1 < p < 6. \tag{11}$$

$$\left\|\Delta\rho^\varepsilon\right\|^2 \le C < \infty. \tag{12}$$

We obtain Equation 13 based on Equation 7, and then evaluate similarly in the negative norm p^ε and obtain inequality (14).

$$\rho^\varepsilon \in L_p(Q), 1 < p < 6. \tag{13}$$

$$\left\|p^\varepsilon\right\| \le C\left\|\nabla p^\varepsilon\right\| < \infty. \tag{14}$$

2) We proceed to the second stage, Galerkin's method, to construct approximate solutions.

Let be $\{\theta_i\}$ is basis in space $L_2(Q)$ for system (15):

$$\begin{cases} \gamma\Delta\theta_i - \nabla p_i = \kappa_i\theta_i \\ \varepsilon p_i + div\,\theta_i = 0 \\ \theta_i\big|_\Gamma = 0. \end{cases} \tag{15}$$

The approximate solutions $\upsilon^{N,\varepsilon}, \rho^{N,\varepsilon}, p^{N,\varepsilon}$ are presented in the form of (16), (17), and (18). Density and pressure are classic solutions to problems (17) and (18), respectively.

$$\upsilon^{N,\varepsilon} = \sum_{i=1}^{N}\tau_i^N\theta_i. \tag{16}$$

$$\begin{cases} \left(\upsilon^{N,\varepsilon}\cdot\nabla\right)\rho^{N,\varepsilon} = \kappa\Delta\rho^{N,\varepsilon} \\ \rho^{N,\varepsilon}\big|_\Gamma = \rho_\Gamma(x) \end{cases} \tag{17}$$

$$\varepsilon p^{N,\varepsilon} + div\,\upsilon^{N,\varepsilon} = 0. \tag{18}$$

Numbers τ_i^N are from the system of Equations 19:

$$\left(\rho^{N,\varepsilon}\left(\upsilon^{N,\varepsilon}\cdot\nabla\right)\upsilon^{N,\varepsilon} - \gamma\Delta\upsilon^{N,\varepsilon} - \kappa\left(\nabla\rho^{N,\varepsilon}\cdot\nabla\right)\upsilon^{N,\varepsilon} - \kappa\left(\upsilon^{N,\varepsilon}\cdot\nabla\right)\rho^{N,\varepsilon} + \right.$$
$$\left. + \kappa^2 div\left(\left(\frac{1}{\rho^{N,\varepsilon}}\cdot\nabla\rho^{N,\varepsilon}\cdot\nabla\right)\rho^{N,\varepsilon}\right) - \frac{1}{2}\rho^{N,\varepsilon}\upsilon^{N,\varepsilon}div\,\upsilon^{N,\varepsilon}, \theta_i\right) = 0. \tag{19}$$

$i = \overline{1, N}$.

3) Further, by analogy with Reddy, et al. [5]; Kazhikenova, et al. [6]; Ladijenskaya [7]; Skorokhodov and Kuzmina [15]; Iskakova, et al. [16] and Kazhikenova, et al. [26] using Brauer's lemma, we prove the existence of a solution to problems (16) – (18) and show that for approximate solutions $\upsilon^{N,\varepsilon}, \rho^{N,\varepsilon}, p^{N,\varepsilon}$, a priori estimates are fair for

approximate solutions (7), (9), (11) – (14). Then, from the sequences $\{\upsilon^{N,\varepsilon}\},\{\rho^{N,\varepsilon}\},\{p^{N,\varepsilon}\}$, can identify the subsequences for which it is true.

$\rho^{N,\varepsilon} \to \rho^{\varepsilon}$ and $\frac{1}{\rho^{N,\varepsilon}} \to \frac{1}{\rho^{\varepsilon}}$ weakly in the $L_{\infty}(Q)$,

$\rho^{N,\varepsilon} \to \rho^{\varepsilon}$ weakly in the $W_2^2(Q), \upsilon^{N,\varepsilon} \to \upsilon^{\varepsilon}$ weakly in the $W_2^1(Q)$,

$p^{N,\varepsilon} \to p^{\varepsilon}$ weakly in the $L_2(Q)$,

$\rho^{N,\varepsilon} \to \rho^{\varepsilon}$ and $\upsilon^{N,\varepsilon} \to \upsilon^{\varepsilon}$ strongly in the $L_p(Q)$, $1 < p \le 6$.

Let us to limit the $\varepsilon \to 0$ of the selected sequences in integral identity corresponding to the integral identity in Definition 1 and in (17) – (18). We conclude that the limit functions $\upsilon^{\varepsilon}, \rho^{\varepsilon}, p^{\varepsilon}$ is a strongly generalized solution to problems (3) and (4).

Assertion 1 is proved.

Assertion 2. *Let all conditions of Proposition 1 are satisfied. Then the strongly generalized solution of system equation (3) - (4) at* $\varepsilon \to 0$ *converges to the strongly generalized solution of original model (1) - (2).*

Proof. The obtained uniform prior estimates establish the convergence of the functions $\upsilon^{\varepsilon}, \rho^{\varepsilon}, p^{\varepsilon}$:

$\frac{1}{\rho^{\varepsilon}} \to \frac{1}{\rho}$ and $\rho^{\varepsilon} \to \rho$ weakly in the $L_{\infty}(Q)$,

$\rho^{\varepsilon} \to \rho$ weakly in the $W_2^2(Q), \upsilon^{\varepsilon} \to \upsilon$ weakly in the, $W_2^1(Q)$

$\rho^{\varepsilon} \to \rho$ and $\upsilon^{\varepsilon} \to \upsilon$ strongly in the $L_p(Q)$, $1 < p \le 6$,

$\varepsilon p^{\varepsilon} \to 0$ strongly in the $L_2(Q)$.

Let us consider the limit of $\varepsilon \to 0$ for the corresponding integral identities. We conclude that the limit functions υ, p, ρ are strongly generalized solutions to the original model systems (1) – (2).

Assertion 2 is proved.

3. Results and Discussion

The main task faced by modern metallurgists is to obtain high-quality products with an ever-increasing demand from machine builders while minimizing the costs of their production. One of the most effective ways to solve these problems is through the comprehensive development of production process technologies [27-32].

The author proposes a new method for the calculation of the hydraulic resistance of channels with a constant cross-section. This method is based on estimates obtained for the average energy dissipation rate in turbulent flow. The proposed method allows for the calculation of the hydraulic resistance of various channels with sufficiently high accuracy and is based only on information about the channel geometry [33]. Modern achievements in this area have made it possible to master the production of copper rods of high quality at the «Kazakhmys Corporation» LLP. Section 3 presents the results of the numerical simulation of metal melt motion under changing physical characteristics of the melt and the design features of industrial equipment at the «Kazakhmys Corporation» LLP.

Currently, modelling methods are widely used to solve a number of complex scientific and technical problems. This is because the solution to many problems, including metallurgical problems, in full-scale conditions for a number of reasons (opacity and high temperature of metal, cumbersome and expensive installation, and aggressive properties of molten metal) is quite difficult.

The modelling of momentum transfer processes requires geometric, kinematic, and dynamic similarities [34-40]. This implies that the model and nature should be similar, the dimensionless velocity fields in the considered flows should be the same, and the differential equations of motion and boundary conditions should be similar. Copper and its alloys are important non-ferrous metals that are widely used in many environments and industries [35, 41-48].

The metal melt moved along the inclined chute of the metallurgical equipment. The physical and mathematical model of this technological process is built under the assumption that the length of the trough is infinite, and the metal melt moves along the axis of the trough in such a way that of the three components $u, \upsilon, \omega,$ of velocity only one component $w,$ remains. As a result, we obtained a model with isothermal motion of the melt in which the density ρ and viscosity λ are constant. In the process of copper alloy hot continuous rolling, the problem of copper sticking to the chute significantly affects the quality of copper products. This study aims to address the problem of copper sticking to the chute during the hot rolling process by investigating the key technologies intended to improve the production line process of copper rods.

Let us consider the physical and mathematical model of incompressible melt motion in the absence of electromagnetic fields but in the presence of mass gravity. The melt motion is described by the Navier-Stokes equation:

$$\begin{cases} -\frac{1}{\rho}\frac{\partial p}{\partial x}=0, \\ -\frac{1}{\rho}\frac{\partial p}{\partial y}=0, \\ \omega\frac{\partial \omega}{\partial z}=-\frac{1}{\rho}\frac{\partial p}{\partial z}+\xi\left(\frac{\partial^2\omega}{\partial x^2}+\frac{\partial^2\omega}{\partial y^2}+\frac{\partial^2\omega}{\partial z^2}\right), \\ \frac{\partial \omega}{\partial z}=0. \end{cases} \quad (20)$$

The velocity function ω depends only on the variable x, y whereas the pressure function depends on the z coordinates. The change in pressure from section to section was negligible and maintained the same value in a given section. Such motions are called steady-state motions. The right side of (21) depends on the x, y coordinates, whereas the right side depends on the z coordinates.

$$\frac{dp}{dz}=\lambda\left(\frac{\partial^2\omega}{\partial x^2}+\frac{\partial^2\omega}{\partial y^2}\right). \quad (21)$$

The main statement of hydrodynamics is $\frac{dp}{dz}=-\frac{\Delta p}{\ell}$, ℓ is the chute length.

When the melt moves along the inclined chute of metallurgical equipment, there is a free surface of the metal melt; therefore, the pressure will be equal to atmospheric pressure. The angle of inclination of the chute to the horizontal surface is equal to Θ, there is a volumetric force, the projection of which on the axis Oz is equal to $F_z=\lambda\sin\Theta=\frac{\Delta p}{\ell}$. We obtain Equation 22.

$$\lambda\left(\frac{\partial^2\omega}{\partial x^2}+\frac{\partial^2\omega}{\partial y^2}\right)+\rho\lambda\sin\Theta=0. \quad (22)$$

$$\omega=0 \text{ at } y=0,\ \frac{\partial\omega}{\partial y}=0 \text{ at } y=\lambda_1,\quad \frac{\partial\omega}{\partial x}=0 \text{ at } x=\lambda_2. \quad (23)$$

The boundary conditions for the system (20) are determined by the equation of adhesion of the metal melt to the walls of the bottom trough as well as by the absence of friction on the free surface of the melt. The depth of the melt flow is equal to λ_1, the width of the melt flow is equal to λ_2. The system of Equations (22) – (23) represents the boundary conditions of this boundary value problem. The physical and mathematical models (22) – (23) are constructed for the technological equipment SCR PROCESS. The technological scheme of the equipment, the cross-section of the equipment bottom chute, and level of metal melt in the bottom chute are shown in Figure 2. Calculations were performed for the lower chute with an inclination angle of 3º. We calculated the numerical values of the melt flow parameters for the SCR PROCESS copper rod line of the «Kazakhmys Corporation» LLP business perimeter $\Omega=\frac{\left[\ell r-\sigma\left(r-\lambda\right)\right]}{2}$, ℓ is arc length, σ is chord, $\lambda-$ is segment arrow: $\sigma=80[\text{mm}],\quad h=16[\text{mm}],\quad \ell\approx\sqrt{\sigma^2+\left(15\lambda^2/3\right)}=\sqrt{80^2+\left(15\cdot16^2/3\right)}=87,6[\text{mm}].$

$$S=\frac{\left[87,6\cdot\frac{104}{2}-80\left(\frac{104}{2}-16\right)\right]}{2}=1675,2[\text{mm}^2].$$

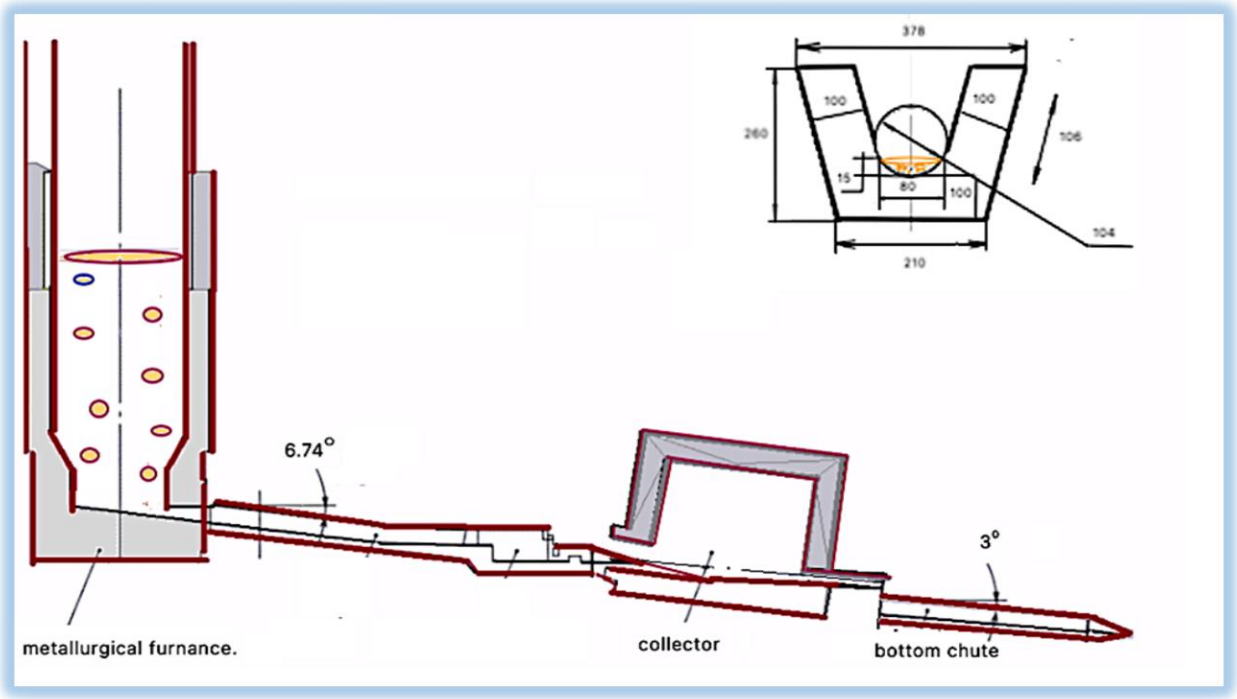

Figure 1.
Technological scheme at the SCR process equipment, measurements are given in [mm].

The average flow velocity of the metal melt is calculated by us according to the formula and is equal to $\upsilon_{mid} \approx 0,43\left[\frac{\text{m}}{\text{s}}\right]$. We used constant time step sizes at the numerical scheme in the calculations $\Delta t = 0,001$, $\Delta x = \Delta y = 0,022$. Then the second melt flow velocity $Q = 3,6\left[\frac{\text{kg}}{\text{s}}\right]$ is determined. The adequacy of our calculations demonstrates the effectiveness of the physical and mathematical models and their application to the calculation of the flow of metallic melts at sufficiently low Reynolds numbers.

The melting parameters include the melt level in the chute, melt temperature, shape of the chute, and angle of inclination to the horizontal. As a result, it was possible to achieve a velocity profile and the presence of vortices during the melt flow. Let us consider the motion of the copper melt, considering shear and bulk viscosities. The copper flow velocity distribution profiles in the lower trough at 1358 [K], 1398 [K], 1438 [K], 1478 [K], 1518 [K], 1558 [K], 1598 [K], and 1638 [K] in the plane in projections on XOY as well as in space in the XYZ coordinate system are presented in Figure 1 and Tables 1-8.

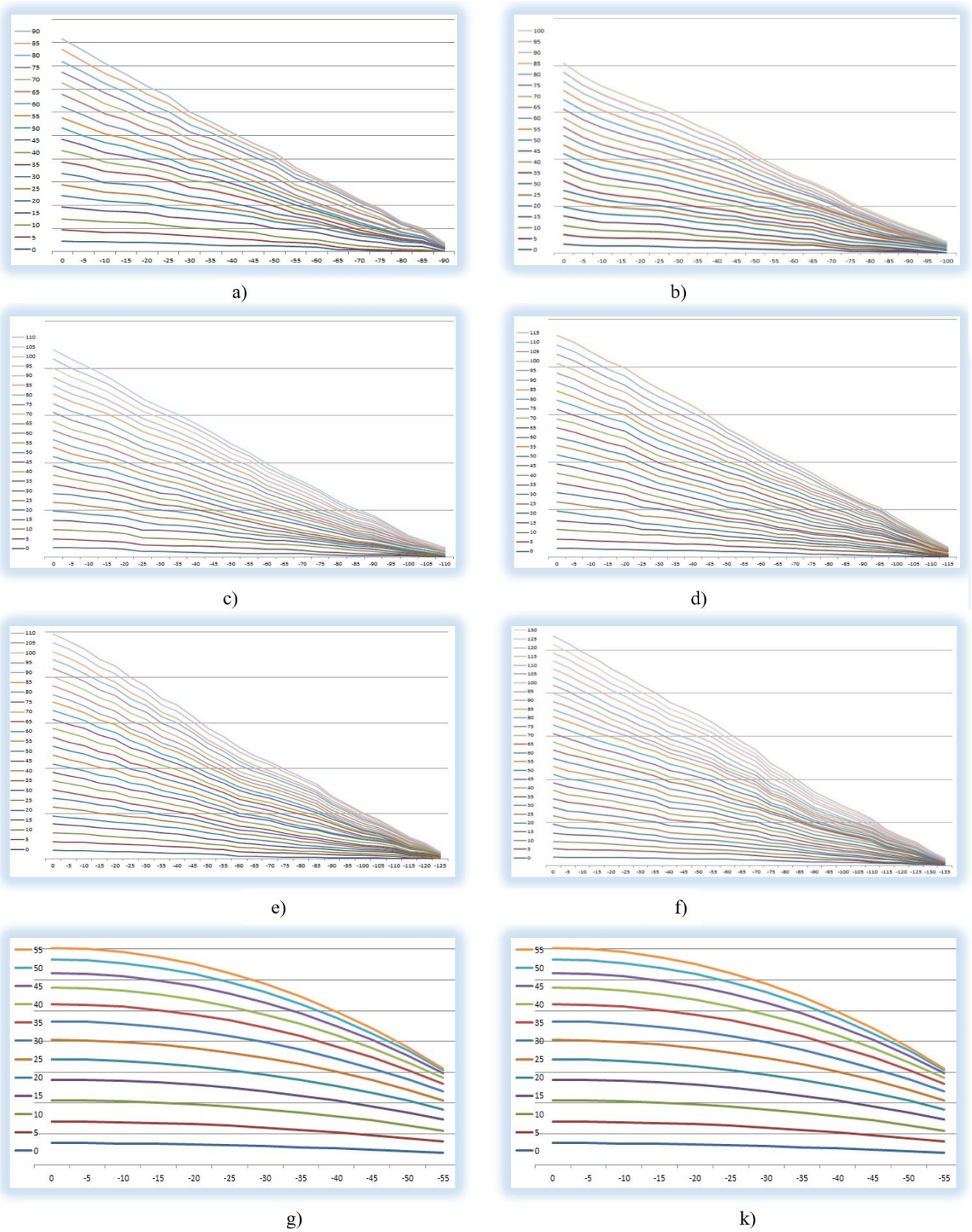

Figure 2.
The copper melt velocity isolines at a)1358 [K], b)1398 [K], c)1438 [K], d)1478 [K], e)1518 [K], f)1558 [K], g)1598 [K], k)1638 [K] temperatures.

Table 1.
The Copper Melt Velocity Profiles at 1358 [K].

X/Y	0.0000	5.000	10.000	15.000	20.000	25.000	30.000	35.000	40.000	45.000	50.000
0.0000	0.4020	0.4000	0.3960	0.3890	0.3770	0.3630	0.3460	0.3260	0.3030	0.2760	0.2470
- 5.00	0.4000	0.3990	0.3940	0.3870	0.3760	0.3620	0.3450	0.3240	0.3010	0.2750	0.2460
-10.00	0.3930	0.3940	0.3900	0.3820	0.3720	0.3570	0.3400	0.3200	0.2970	0.2700	0.2410
-15.00	0.3850	0.3870	0.3820	0.3740	0.3630	0.3490	0.3320	0.3120	0.2890	0.2630	0.2330
-20.00	0.3770	0.3760	0.3710	0.3630	0.3520	0.3380	0.3210	0.3010	0.2780	0.2520	0.2220
-25.00	0.3630	0.3620	0.3570	0.3490	0.3380	0.3250	0.3070	0.2870	0.2640	0.2380	0.2080
-30.00	0.3460	0.3450	0.3400	0.3320	0.3210	0.3070	0.2910	0.2700	0.2470	0.2210	0.1920
-35.00	0.3260	0.3240	0.3200	0.3120	0.3010	0.2870	0.2700	0.2510	0.2270	0.2020	0.1710
-40.00	0.3030	0.3010	0.2970	0.2890	0.2780	0.2640	0.2470	0.2270	0.2050	0.1770	0.1480
-45.00	0.2760	0.2750	0.2700	0.2630	0.2520	0.2380	0.2210	0.2010	0.1770	0.1510	0.1220
-50.00	0.2470	0.2460	0.2410	0.2330	0.2220	0.2080	0.1910	0.1710	0.1480	0.1220	0.0920

Table 2.
The Copper Melt Velocity Profiles at 1398 [K].

X/Y	0.0000	5.000	10.000	15.000	20.000	25.000	30.000	35.000	40.000	45.000	50.000
0.0000	0.4420	0.4390	0.4340	0.4250	0.4140	0.3980	0.3800	0.3580	0.3320	0.3030	0.2710
- 5.00	0.4390	0.4380	0.4320	0.4240	0.4120	0.3970	0.3780	0.3560	0.3300	0.3020	0.2690
-10.00	0.4340	0.4320	0.4280	0.4190	0.4070	0.3910	0.3730	0.3510	0.3250	0.2960	0.2640
-15.00	0.4250	0.4240	0.4190	0.4110	0.3980	0.3830	0.3640	0.3420	0.3170	0.2880	0.2560
-20.00	0.4140	0.4120	0.4070	0.3980	0.3870	0.3710	0.3520	0.3300	0.3050	0.2760	0.2440
-25.00	0.3980	0.3970	0.3910	0.3830	0.3710	0.3570	0.3370	0.3150	0.2900	0.2610	0.2290
-30.00	0.3800	0.3780	0.3730	0.3640	0.3520	0.3370	0.3190	0.2960	0.2710	0.2420	0.2100
-35.00	0.3580	0.3560	0.3510	0.3420	0.3300	0.3150	0.2970	0.2750	0.2490	0.2200	0.1880
-40.00	0.3320	0.3300	0.3250	0.3170	0.3050	0.2900	0.2710	0.2490	0.2240	0.1950	0.1620
-45.00	0.3030	0.3020	0.2960	0.2880	0.2760	0.2610	0.2420	0.2200	0.1950	0.1670	0.1340
-50.00	0.2710	0.2690	0.2640	0.2560	0.2440	0.2290	0.2100	0.1880	0.1620	0.1340	0.1020

Table 3.
The Copper Melt Velocity Profiles at 1438 [K].

X/Y	0.0000	5.000	10.000	15.000	20.000	25.000	30.000	35.000	40.000	45.000	50.000
0.0000	0.4820	0.4790	0.4740	0.4640	0.4510	0.4350	0.4140	0.3900	0.3620	0.3310	0.2960
- 5.00	0.4790	0.4780	0.4720	0.4620	0.4490	0.4330	0.4120	0.3880	0.3610	0.3290	0.2940
-10.00	0.4740	0.4720	0.4670	0.4570	0.4440	0.4270	0.4070	0.3830	0.3550	0.3240	0.2880
-15.00	0.4640	0.4620	0.4570	0.4490	0.4350	0.4180	0.3980	0.3740	0.3460	0.3140	0.2790
-20.00	0.4510	0.4490	0.4440	0.4350	0.4230	0.4050	0.3850	0.3610	0.3330	0.3010	0.2660
-25.00	0.4350	0.4330	0.4270	0.4180	0.4050	0.3890	0.3680	0.3440	0.3160	0.2850	0.2490
-30.00	0.4140	0.4120	0.4070	0.3980	0.3850	0.3680	0.3490	0.3240	0.2960	0.2640	0.2290
-35.00	0.3900	0.3880	0.3830	0.3740	0.3610	0.3440	0.3240	0.2990	0.2720	0.2400	0.2050
-40.00	0.3620	0.3610	0.3550	0.3460	0.3330	0.3160	0.2960	0.2730	0.2440	0.2120	0.1770
-45.00	0.3310	0.3290	0.3240	0.3140	0.3010	0.2850	0.2640	0.2400	0.2130	0.1820	0.1460
-50.00	0.2960	0.2940	0.2880	0.2790	0.2660	0.2490	0.2290	0.2050	0.1770	0.1460	0.1120

Table 4.
The Copper Melt Velocity Profiles at 1478 [K].

X/Y	0.0000	5.000	10.000	15.000	20.000	25.000	30.000	35.000	40.000	45.000	50.000
0.0000	0.5230	0.5200	0.5140	0.5040	0.4900	0.4720	0.4500	0.4240	0.3940	0.3590	0.3210
- 5.00	0.5200	0.5190	0.5120	0.5020	0.4880	0.4700	0.4480	0.4220	0.3920	0.3570	0.3190
-10.00	0.5140	0.5120	0.5070	0.4960	0.4820	0.4640	0.4420	0.4160	0.3860	0.3510	0.3130
-15.00	0.5040	0.5020	0.4960	0.4870	0.4720	0.4540	0.4320	0.4060	0.3750	0.3410	0.3030
-20.00	0.4900	0.4880	0.4820	0.4720	0.4590	0.4400	0.4180	0.3920	0.3610	0.3270	0.2890
-25.00	0.4720	0.4700	0.4640	0.4540	0.4400	0.4230	0.4000	0.3730	0.3430	0.3090	0.2710
-30.00	0.4500	0.4480	0.4420	0.4320	0.4180	0.4010	0.3780	0.3510	0.3210	0.2870	0.2490
-35.00	0.4240	0.4220	0.4160	0.4060	0.3920	0.3790	0.3510	0.3260	0.2950	0.2610	0.2230
-40.00	0.3940	0.3920	0.3860	0.3790	0.3610	0.3370	0.3210	0.2950	0.2660	0.2310	0.1920
-45.00	0.3590	0.3570	0.3510	0.3410	0.3270	0.3090	0.2870	0.2610	0.2310	0.1970	0.1580
-50.00	0.3210	0.3190	0.3130	0.3030	0.2890	0.2710	0.2490	0.2230	0.1920	0.1580	0.1210

Table 5.
The Copper Melt Velocity Profiles at 1518 [K].

X/Y	0.0000	5.000	10.000	15.000	20.000	25.000	30.000	35.000	40.000	45.000	50.000
0.0000	0.5660	0.5200	0.5630	0.5560	0.5300	0.5110	0.4870	0.4580	0.4260	0.3890	0.3470
- 5.00	0.5630	0.5190	0.5610	0.5540	0.5280	0.5080	0.4850	0.4560	0.4240	0.3870	0.3450
-10.00	0.5560	0.5120	0.5550	0.5480	0.5210	0.5020	0.4780	0.4500	0.4170	0.3800	0.3390
-15.00	0.5450	0.5020	0.5430	0.5380	0.5110	0.4910	0.4670	0.4390	0.4060	0.3690	0.3280
-20.00	0.5300	0.4880	0.5280	0.5210	0.4960	0.4760	0.4520	0.4240	0.3910	0.3540	0.3130
-25.00	0.5110	0.4700	0.5080	0.5020	0.4760	0.4570	0.4320	0.4040	0.3710	0.3340	0.2930
-30.00	0.4870	0.4480	0.4850	0.4780	0.4520	0.4320	0.4090	0.3800	0.3470	0.3100	0.2690
-35.00	0.4580	0.4220	0.4560	0.4500	0.4240	0.4040	0.3800	0.3530	0.3190	0.2820	0.2410
-40.00	0.4260	0.3920	0.4240	0.4170	0.3910	0.3710	0.3470	0.3190	0.2880	0.2500	0.2080
-45.00	0.3890	0.3570	0.3870	0.3800	0.3540	0.3340	0.3100	0.2820	0.2500	0.2140	0.1710
-50.00	0.3470	0.3190	0.3450	0.3390	0.3130	0.2930	0.2690	0.2410	0.2080	0.1710	0.1310

Table 6.
The Copper Melt Velocity Profiles at 1558 [K].

X/Y	0.0000	5.000	10.000	15.000	20.000	25.000	30.000	35.000	40.000	45.000	50.000
0.0000	0.6110	0.6070	0.6000	0.5890	0.5720	0.5510	0.5250	0.4950	0.4590	0.4200	0.3750
- 5.00	0.6070	0.6060	0.5980	0.5860	0.5700	0.5490	0.5230	0.4920	0.4570	0.4170	0.3730
-10.00	0.6000	0.5980	0.5920	0.5790	0.5630	0.5420	0.5160	0.4850	0.4500	0.4100	0.3660
-15.00	0.5890	0.5860	0.5790	0.5680	0.5510	0.5300	0.5040	0.4740	0.4380	0.3980	0.3540
-20.00	0.5720	0.5700	0.5630	0.5510	0.5360	0.5130	0.4880	0.4570	0.4220	0.3820	0.3370
-25.00	0.5510	0.5490	0.5420	0.5300	0.5130	0.4930	0.4660	0.4360	0.4010	0.3610	0.3160
-30.00	0.5250	0.5230	0.5160	0.5040	0.4880	0.4660	0.4420	0.4100	0.3750	0.3350	0.2900
-35.00	0.4950	0.4920	0.4850	0.4740	0.4570	0.4360	0.4100	0.3810	0.3450	0.3050	0.2600
-40.00	0.4590	0.4570	0.4500	0.4380	0.4220	0.4010	0.3750	0.3440	0.3090	0.2690	0.2250
-45.00	0.4200	0.4170	0.4100	0.3980	0.3820	0.3610	0.3350	0.3050	0.2690	0.2290	0.1850
-50.00	0.3750	0.3730	0.3660	0.3540	0.3370	0.3160	0.2900	0.2600	0.2250	0.1860	0.1410

Table 7.
The Copper Melt Velocity Profiles at 1598[K].

X/Y	0.0000	5.000	10.000	15.000	20.000	25.000	30.000	35.000	40.000	45.000	50.000
0.0000	0.6010	0.6510	0.6430	0.6310	0.6130	0.5910	0.5630	0.5300	0.4920	0.4500	0.4020
- 5.00	0.6510	0.6490	0.6410	0.6280	0.6110	0.5880	0.5600	0.5280	0.4900	0.4470	0.3990
-10.00	0.6430	0.6410	0.6340	0.6210	0.6030	0.5800	0.5530	0.5200	0.4820	0.4400	0.3920
-15.00	0.6310	0.6280	0.6210	0.6090	0.5910	0.5680	0.5400	0.5070	0.4700	0.4270	0.3790
-20.00	0.6130	0.6110	0.6030	0.5910	0.5740	0.5500	0.5230	0.4900	0.4520	0.4090	0.3620
-25.00	0.5910	0.5880	0.5800	0.5680	0.5500	0.5290	0.5000	0.4670	0.4300	0.3870	0.3390
-30.00	0.5630	0.5600	0.5530	0.5400	0.5230	0.5000	0.4730	0.4400	0.4020	0.3590	0.3110
-35.00	0.5300	0.5280	0.5200	0.5070	0.4900	0.4670	0.4400	0.4080	0.3690	0.3260	0.2790
-40.00	0.4920	0.4900	0.4820	0.4700	0.4520	0.4300	0.4020	0.3690	0.3330	0.2890	0.2410
-45.00	0.4500	0.4470	0.4400	0.4270	0.4090	0.3870	0.3590	0.3260	0.2890	0.2470	0.1980
-50.00	0.4020	0.3990	0.3920	0.3790	0.3620	0.3390	0.3110	0.2790	0.2410	0.1980	0.1510

Table 8.
The Copper Melt Velocity Profiles at 1638 [K].

X/Y	0.0000	5.000	10.000	15.000	20.000	25.000	30.000	35.000	40.000	45.000	50.000
0.0000	0.6990	0.6970	0.6880	0.6750	0.6560	0.6320	0.6020	0.5670	0.5270	0.4810	0.4300
- 5.00	0.6970	0.6940	0.6870	0.6720	0.6530	0.6290	0.5990	0.5640	0.5240	0.4780	0.4270
-10.00	0.6880	0.6860	0.6770	0.6640	0.6450	0.6210	0.5910	0.5560	0.5160	0.4700	0.4190
-15.00	0.6750	0.6720	0.6640	0.6520	0.6330	0.6070	0.5780	0.5430	0.5030	0.4570	0.4060
-20.00	0.6560	0.6530	0.6450	0.6320	0.6130	0.5890	0.5590	0.5240	0.4840	0.4380	0.3870
-25.00	0.6320	0.6290	0.6210	0.6070	0.5890	0.5650	0.5350	0.5000	0.4590	0.4140	0.3630
-30.00	0.6020	0.5990	0.5910	0.5780	0.5590	0.5350	0.5060	0.4700	0.4300	0.3840	0.3330
-35.00	0.5670	0.5640	0.5560	0.5430	0.5240	0.5000	0.4700	0.4360	0.3950	0.3490	0.2980
-40.00	0.5270	0.5240	0.5160	0.5030	0.4840	0.4590	0.4300	0.3950	0.3560	0.3090	0.2580
-45.00	0.4810	0.4780	0.4700	0.4570	0.4380	0.4140	0.3840	0.3490	0.3090	0.2640	0.2120
-50.00	0.4300	0.4270	0.4190	0.4060	0.3870	0.3630	0.3330	0.2980	0.2580	0.2120	0.1620

The physical picture of the copper melt flow in the process equipment is as follows: the different layers of melt do not mix with each other when traveling down the trough. The melt represents separate layers that move towards the melt surface at different velocities. From the moment atoms jump in the direction of the volumetric force, the flow is separated into a bottom layer and a main layer. The atoms of the bottom layer are held near the bottom surface by interatomic coupling forces, whereas those of the main layer move along the boundary of the bottom layer under the action of the bulk force. The walls of the trough, due to internal friction, inhibit the movement of the nearest copper melt layer, and this inhibition is transmitted from one layer to another throughout the melt flow to the surface, where the flow is the fastest» [9].

The maximum isoline value was observed at 1558 [K] and are presented in Figure 3 and Table 9.

Table 9.
The Maximum Isoline Value of the Velocity at the Specified Temperatures.

T [K]	1358	1398	1438	1478	1518	1558	1598	1638
n is number of isolines	19	22	23	26	27	28	14	12

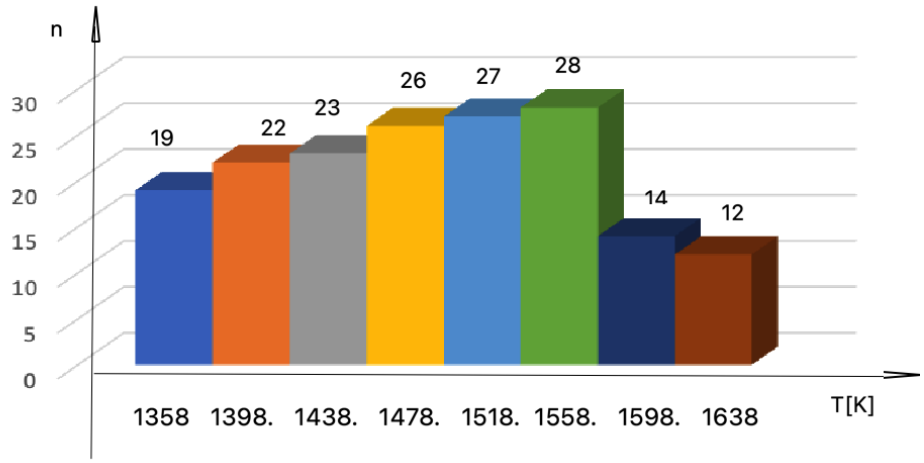

Figure 3.
The maximum isoline value of the velocity at the specified temperatures.

The distribution of isolines was not dense at lower temperatures, for example, at 1358 [K], or at higher temperatures, for example, at 1598 [K]. The calculations indicated inhomogeneity of the melt near the melting temperature, which confirmed the presence of a melt cluster structure. Calculations also indicate inhomogeneity at 1598 [K] and above, which is due to thermal loosening of the metallic melt structure and is the cause of mechanical defects in obtaining the intermediate product.

Verification of theoretical results with practical results for SCR PROCESS copper rod line of the «Kazakhmys Corporation» LLP shows the adequacy of our mathematical model, its objectivity and reliability.

Velocity isolines vary from $0,64\left[\frac{\text{m}}{\text{s}}\right]$ to $0,01\left[\frac{\text{m}}{\text{s}}\right]$. In the mathematical model of melt motion, the maximum velocity of melt motion is reached at the surface, which is practically equal to zero at the bottom of the trough. This is consistent with the boundary conditions of Equations (19) and (20). The calculations show that the average value of the isoline velocity is approximately equal to the average velocity of the copper melt flow $\upsilon \approx 0,4\left[\frac{\text{m}}{\text{s}}\right]$. Let we calculate the number of isolines at the specified temperatures.

The temperature of the copper melt flow in the process equipment was theoretically calculated using numerical methods. The correctness and adequacy of our calculations were confirmed by verification with real temperatures of copper melt movement in the range of 1425-1558 [K], which are close to the temperatures in industrial conditions.

4. Conclusion

- In a limited area $Q \in R^3$ with smooth border $\Gamma = \partial Q$ we consider nonlinear stationary equations representing a mathematical model of the incompressible melt motion. We justify the limit transition from the solutions of the Navier-Stokes approximating system equations to the original system. The solution of the approximate problem (3) – (4) at $\varepsilon \to 0$ is a strongly generalized solution of the original problems (1) – (2). The proof consists of three stages: obtaining a priori estimates using Galerkin's method, and limit transfer. The systems described by the Navier-Stokes equations and having certain boundary conditions (pressures or velocities) at all boundaries were closed. Such systems include those bounded by impermeable walls, free surfaces under a known pressure, and movable walls under a known pressure.

- A numerical scheme for the regularization of the boundary value problems of incompressible fluid motion equations was developed. The complexity of solving these problems lies in the fact that the system of differential equations is non-evolutionary. The incompressible melt motion equation does not contain the time derivative of the pressure function. By introducing a small parameter in the original equation, the time derivative of the pressure function can be transformed from a non-evolutionary system of equations to an evolutionary system. Convergence of the solution of the approximation problem to the original boundary value problem of metallic melt motion was established.
- The verification of theoretical results with practical ones allowed the development of a mathematical model of melt motion and the numerical integration algorithm of hydrodynamic equations, which will enable the prediction of technological parameters of casting to produce high-quality products.
- The validation of the obtained theoretical results with real parameters of copper melt movement in the process equipment for the SCR PROCESS copper rod line confirmed the validity and reliability of our research. The correctness and adequacy of our calculations were confirmed by verification with real temperatures of copper melt movement in the range of 1425-1558 [K], which are close to the temperatures in industrial conditions. The calculations show that the average value of the isoline velocity is approximately equal to the average velocity of the copper melt for the SCR PROCESS copper rod line of the Kazakhmys Corporation LLP. The results show that the best melting occurred at 1558 [K].

References

[1] K. Urbanowicz, A. Bergant, M. Stosiak, A. Deptuła, and M. Karpenko, "Navier-stokes solutions for accelerating pipe flow—a review of analytical models," *Energies*, vol. 16, no. 3, p. 1407, 2023. https://doi.org/10.3390/en16031407

[2] V. V. Lasukov, "Cosmological and quantum solutions of the navier–stokes equations," *Russian Physics Journal*, vol. 62, no. 5, pp. 778-793, 2019. https://doi.org/10.1007/s11182-019-01778-w

[3] S. S. Kazhikenova, "The unique solvability of stationary and non-stationary incompressible melt models in the case of their linearization," *Archives of Control Sciences*, vol. 31, no. 2, pp. 307-332, 2021. https://doi.org/10.24425/acs.2021.137420

[4] D. Zhao, "Quick finite volume solver for incompressible Navier-Stokes equation by parallel Gram-Schmidt process based GMRES and HSS," *Engineering Computations*, vol. 32, no. 5, pp. 1460-1476, 2015. https://doi.org/10.1108/ec-02-2014-0032

[5] M. H. L. Reddy, S. K. Dadzie, R. Ocone, M. K. Borg, and J. M. Reese, "Recasting Navier–Stokes equations," *Journal of Physics Communications*, vol. 3, no. 10, p. 105009, 2019. https://doi.org/10.1088/2399-6528/ab4b86

[6] S. S. Kazhikenova, S. N. Shaltakov, D. Belomestny, and G. S. Shaihova, "Finite difference method implementation for numerical integration of hydrodynamic equations for melts," *Eurasian Physical Technical Journal*, vol. 33, no. 1, pp. 50–56, 2020.

[7] O. Ladijenskaya, *Boundary value problems of mathematical physics*. Moscow: Nauka, 1973.

[8] S. S. Kazhikenova, S. N. Shaltakov, and B. R. Nussupbekov, "Difference melt model," *Archives of Control Sciences*, vol. 31, no. 3, pp. 607–627, 2021. https://doi.org/10.24425/acs.2021.138694

[9] A. Abramov and L. F. Yukhno, "Solving some problems for systems of linear ordinary differential equations with redundant conditions," *Zhurnal Vychislitel'noi Matematiki i Matematicheskoi Fiziki*, vol. 57, no. 8, pp. 1285–1293, 2017. https://doi.org/10.7868/S0044466917080026

[10] D. Samantaray and M. K. Das, "Nature of turbulence inside a cubical lid-driven cavity: Effect of Reynolds number," *International Journal of Heat and Fluid Flow*, vol. 80, p. 108498, 2019. https://doi.org/10.1016/j.ijheatfluidflow.2019.108498

[11] F. Picella, J. C. Loiseau, F. Lusseyran, J. C. Robinet, S. Cherubini, and L. Pastur, "Successive bifurcations in a fully three-dimensional open cavity flow," *Journal of Fluid Mechanics*, vol. 844, pp. 855-877, 2018. https://doi.org/10.1017/jfm.2018.169

[12] X. Yan *et al.*, "Numerical simulation of meso-micro structure in ni-based superalloy during liquid metal cooling process," in *Proceedings of the 4th World Congress on Integrated Computational Materials Engineering (ICME 2017) (pp. 249-259). Cham: Springer International Publishing*, 2017.

[13] T. A. Barannyk, A. F. Barannyk, and I. I. Yuryk, "Exact solutions of the nonlinear equation," *Ukrains'kyi Matematychnyi Zhurnal*, vol. 69, no. 9, pp. 1180–1186, 2017.

[14] A. Felipe, R. Sevilla, and O. Hassan, "A conservative degree adaptive HDG method for transient incompressible flows," *International Journal of Numerical Methods for Heat & Fluid Flow*, vol. 35, no. 1, pp. 300-329, 2024. https://doi.org/10.1108/hff-09-2024-0651

[15] S. L. Skorokhodov and N. P. Kuzmina, "Analytical-numerical method for solving an Orr–Sommerfeld-type problem for analysis of instability of ocean currents," *Zh. Vychisl. Mat. Mat. Fiz.*, vol. 58, no. 6, pp. 1022–1039, 2018. https://doi.org/10.7868/S0044466918060133

[16] N. Iskakova, A. Assanova, and E. Bakirova, "Numerical method for the solution of linear boundary-value problem for integrodifferential equations based on spline approximations," *Ukrains' kyi Matematychnyi Zhurnal*, vol. 71, no. 9, pp. 1176-1191, 2019.

[17] A. M. Molchanov, *Numerical methods for solving the Navier-Stokes equations*. Moscow: Nauka, 2018.

[18] M. P. Carvalho, V. L. Scalon, and A. Padilha, "Analysis of CBS numerical algorithm execution to flow simulation using the finite element method," *Ingeniare. Revista chilena de Ingeniería*, vol. 17, no. 2, pp. 166–174, 2009. https://doi.org/10.4067/S0718-33052009000200005

[19] F. H. Ali, M. F. Almensoury, A. S. Hashim, Q. R. Al-Amir, H. K. Hamzah, and M. Hatami, "Nanofluid natural convection of hot concentric cylinder in oval-shaped porous cavity at different eccentricity," *International Journal of Numerical Methods for Heat & Fluid Flow*, vol. 34, no. 5, pp. 2146-2176, 2024. https://doi.org/10.1108/hff-08-2023-0494

[20] C. A. Bayona Roa, J. Baiges, and R. Codina, "Variational multi-scale finite element approximation of the compressible Navier-Stokes equations," *International Journal of Numerical Methods for Heat & Fluid Flow*, vol. 26, no. 3-4, pp. 1240-1271, 2016. https://doi.org/10.1108/hff-11-2015-0483

[21] K. K. Ranjan, S. Kumar, A. Tyagi, and A. Sharma, "An adaptive wavelet Galerkin scheme for solving contact problems based on elliptic variational inequalities of the first kind," *Engineering Computations*, vol. 36, no. 4, pp. 1258-1281, 2019. https://doi.org/10.1108/ec-07-2018-0294

[22] C. Mao, B. Zhou, and S. Xue, "The actuation performance of a piezoelectric laminated plate actuator via Galerkin method," *Multidiscipline Modeling in Materials and Structures*, vol. 18, no. 5, pp. 900-918, 2022. https://doi.org/10.1108/mmms-05-2022-0086

[23] G. R. Joldes, P. Teakle, A. Wittek, and K. Miller, "Computation of accurate solutions when using element-free Galerkin methods for solving structural problems," *Engineering Computations*, vol. 34, no. 3, pp. 902-920, 2017. https://doi.org/10.1108/ec-01-2016-0017

[24] W. Liu, Z. Huang, and Y. Liu, "An isogeometric analysis approach for solving the Reynolds equation in textured piston ring – cylinder liner contacts," *Engineering Computations*, vol. 37, no. 9, pp. 3045-3078, 2020. https://doi.org/10.1108/ec-03-2019-0076

[25] G. Muratova, T. Martynova, E. Andreeva, V. Bavin, and Z.-Q. Wang, "Numerical solution of the navier–stokes equations using multigrid methods with HSS-Based and STS-based smoothers," *Symmetry*, vol. 12, no. 2, p. 233, 2020. https://doi.org/10.3390/sym12020233

[26] S. S. Kazhikenova, M. I. Ramazanov, A. A. Khairkulova, and G. S. Shaikhova, "ε-Approximation of the temperatures model of inhomogeneous melts with allowance for energy dissipation," *Bulletin of the Karaganda University. Mathematics Series*, vol. 90, no. 2, pp. 93-100, 2018. https://doi.org/10.31489/2018m2/93-100

[27] Y. A. Mayi *et al.*, "Multiphysics simulation of single pulse laser powder bed fusion: comparison of front capturing and front tracking methods," *International Journal of Numerical Methods for Heat & Fluid Flow*, vol. 32, no. 6, pp. 2149-2176, 2021. https://doi.org/10.1108/hff-04-2021-0282

[28] L. Deng, J. Liang, Y. Zhang, H. Zhou, and Z. Huang, "Efficient numerical simulation of injection mold filling with the lattice Boltzmann method," *Engineering Computations*, vol. 34, no. 2, pp. 307-329, 2017. https://doi.org/10.1108/ec-01-2016-0023

[29] H. F. Oztop, M. Gür, F. Selimefendigil, and H. Coşanay, "Analysis of melting of phase change material inserted a block via impinging turbulent slot jet," *International Journal of Numerical Methods for Heat & Fluid Flow*, vol. 33, no. 10, pp. 3467-3491, 2023. https://doi.org/10.1108/hff-03-2023-0109

[30] B. Abbes, T. Anedaf, F. Abbes, and Y. Li, "Direct energy deposition metamodeling using a meshless method," *Engineering Computations*, vol. 38, no. 3, pp. 1226-1240, 2020. https://doi.org/10.1108/ec-10-2019-0447

[31] J. Yang and T. Zhang, "Stability and convergence of iterative finite element methods for the thermally coupled incompressible MHD flow," *International Journal of Numerical Methods for Heat & Fluid Flow*, vol. 30, no. 12, pp. 5103-5141, 2020. https://doi.org/10.1108/hff-11-2019-0821

[32] E. A. Papon, A. Haque, and M. A. R. Sharif, "Numerical study for the improvement of bead spreading architecture with modified nozzle geometries in additive manufacturing of polymers," *Rapid Prototyping Journal*, vol. 27, no. 3, pp. 518-529, 2021. https://doi.org/10.1108/rpj-05-2019-0142

[33] A. Baron, "Determination of hydraulic resistance of channels using spectral geometry methods," *Fluid Dynamics Research*, vol. 53, no. 6, p. 065508, 2021. https://doi.org/10.1088/1873-7005/ac44fa

[34] J. Baumann, T. Siebrecht, and P. Wiederkehr, "Modelling the dynamic behavior of a machine tool considering the tool-position-dependent change of modal parameters in a geometric-kinematic simulation system," *Procedia CIRP*, vol. 62, pp. 351-356, 2017. https://doi.org/10.1016/j.procir.2016.06.077

[35] Y. Liu, Y. Peng, and X. Qu, "Mechanism of and key technologies for copper bonding in the hot rolling of SCR continuous casting and rolling," *Applied Sciences*, vol. 11, no. 22, p. 11023, 2021. https://doi.org/10.3390/app112211023

[36] R. Kumar and P. K. Jha, "Effect of casting speed on solidification and inclusion motions in bloom mold caster under the influence of in-mold electromagnetic stirring," *International Journal of Numerical Methods for Heat & Fluid Flow*, vol. 33, no. 3, pp. 1022-1045, 2022. https://doi.org/10.1108/hff-07-2022-0415

[37] H. He *et al.*, "Fabrication and surface treatment of fine copper lines for HDI printed circuit board with modified full-additive method," *Circuit World*, vol. 43, no. 3, pp. 131-138, 2017. https://doi.org/10.1108/cw-02-2017-0004

[38] M. S. A. Al-Zadi and H. Haghighat, "Experimental evaluation and FE simulation of the asymmetrical rolling process of bimetal rods," *Aircraft Engineering and Aerospace Technology*, vol. 97, no. 4, pp. 488-497, 2025. https://doi.org/10.1108/aeat-10-2024-0302

[39] J. Guan, S. Luo, X. Kan, C. Chen, and Q. Wang, "Preparation of copper/binder composites and fused filament fabrication process," *Rapid Prototyping Journal*, vol. 31, no. 5, pp. 925-933, 2025. https://doi.org/10.1108/rpj-12-2023-0436

[40] M. Hanafi, D. Wibisono, K. Mangkusubroto, M. Siallagan, and M. J. K. Badriyah, "Designing smelter industry investment competitiveness policy in Indonesia through system dynamics model," *Journal of Science and Technology Policy Management*, vol. 10, no. 3, pp. 617-641, 2019. https://doi.org/10.1108/jstpm-06-2018-0064

[41] E. Sharabian *et al.*, "Numerical simulation and analytical modelling of temperature and morphology of melt pool in electron beam powder bed fusion of copper," *Rapid Prototyping Journal*, vol. 31, no. 1, pp. 127-144, 2024. https://doi.org/10.1108/rpj-03-2024-0141

[42] M. H. H. Ishak, M. S. Abdul Aziz, F. Ismail, and M. Z. Abdullah, "Influence of copper pillar bump structure on flip chip packaging during reflow soldering: a numerical approach," *Microelectronics International*, vol. 38, no. 4, pp. 172-181, 2021. https://doi.org/10.1108/mi-05-2021-0044

[43] T. Romano, E. Migliori, M. Mariani, N. Lecis, and M. Vedani, "Densification behaviour of pure copper processed through cold pressing and binder jetting under different atmospheres," *Rapid Prototyping Journal*, vol. 28, no. 6, pp. 1023-1039, 2022. https://doi.org/10.1108/rpj-09-2021-0243

[44] A. Prakash and S. D. Kore, "Wire arc direct energy deposited multiphase steel through in situ micropowder alloying: mechanical and metallurgical studies," *Rapid Prototyping Journal*, vol. 31, no. 1, pp. 62-82, 2024. https://doi.org/10.1108/rpj-02-2024-0094

[45] M. B. Shaik, V. Nasina, and R. S. Mamilla, "Experimental investigation into nano-finishing of pure copper built using atomic diffusion additive manufacturing," *Rapid Prototyping Journal*, vol. 31, no. 5, pp. 998-1013, 2025. https://doi.org/10.1108/rpj-12-2023-0438

[46] H. Adibi and M. R. Hashemi, "Experimental study on tensile strength of copper microparticles filled polymer composites printed by fused deposition modelling process," *Rapid Prototyping Journal*, vol. 28, no. 1, pp. 21-31, 2021. https://doi.org/10.1108/rpj-08-2020-0199

[47] J. Guan, X. Zhang, Y. Jiang, and Y. Yan, "Insights into fabrication mechanism of pure copper thin wall components by selective infrared laser melting," *Rapid Prototyping Journal*, vol. 25, no. 8, pp. 1388-1397, 2019. https://doi.org/10.1108/rpj-06-2018-0143

[48] A. Mezghani, A. R. Nassar, C. J. Dickman, E. Valdes, and R. Alvarado, "Laser powder bed fusion additive manufacturing of copper wicking structures: Fabrication and capillary characterization," *Rapid Prototyping Journal*, vol. 27, no. 6, pp. 1181-1188, 2021. https://doi.org/10.1108/rpj-01-2021-0016